Drag force and transport property of a small cylinder in free molecule flow: A gas-kinetic theory analysis

Changran Liu, Zhigang Li, and Hai Wang

Drag Force and Transport Property of Small Cylinder in Free Molecule Flow: A Gas-Kinetic Theory Analysis

Changran Liu,[1] Zhigang Li,[2] and Hai Wang[1]

[1]*Department of Mechanical Engineering, Stanford University, Stanford, CA 94305, USA*
[2]*Department of Mechanical and Aerospace Engineering, Hong Kong University of Science and Technology, Clear Water Bay, Kowloon, Hong Kong*

Analytical expressions are derived for aerodynamic drag force on small cylinders in the free molecule flow using the gas kinetic theory. The derivation considers the effect of intermolecular interactions between the cylinder and gas media. Two limiting collision models, specular and diffuse scattering, are investigated in two limiting cylinder orientations with respect to the drift velocity. The earlier solution of Dahneke (B. E. Dahneke, Journal of Aerosol Science **4**, 147, 1973) is shown to be a special case of the current expressions in the rigid-body limit of collision. Drag force expressions are obtained for cylinders that undergo Brownian rotation and for those that align with the drift velocity. The validity of the theoretical expressions is tested against experimental mobility data available for carbon nanotubes.

PACS: 47.45.Dt , 51.10.+y, 51.20.+d, 52.25.Fi, 61.46.Fg

I.   INTRODUCTION

Theory of aerodynamic drag force, diffusivity and electric mobility of nanosized slender bodies (NSBs) in a fluid medium is of interest to a wide range of problems. NSBs may include long-chain molecules, nanorods and nanotubes. Applications range from drag on cylinders or chains of spheres [1], size classification of fiberous aerosols [2-6], ion mobility of long-chain molecules and biomolecules [7-9], gas-phase synthesis, separation and characterization of nanotubes and nanorods [10-20], to transport properties of long-chain hydrocarbons in reacting flows [21-23].

Earlier, Batchelor [24] and Cox [25] treated the drag force on a slender body in the Stokes flow region and the low-Reynolds number limit.   For a slender body of radius R and length $\mathcal{L}$ ($2R \ll \mathcal{L}$) undergoing relative motion with a fluid at a drift velocity V, they showed that the drag force takes the forms of

$$F_{\parallel} \cong \frac{2\pi\mu\mathcal{L}}{\ln(\mathcal{L}/R) - 3/2 + \ln 2} V \tag{1}$$

and

$$F_{\perp} \cong \frac{4\pi\mu\mathcal{L}}{\ln(\mathcal{L}/R) - 1/2 + \ln 2} V \ , \tag{2}$$

for cylinder aligned parallel ($\parallel$) and perpendicular ($\perp$) to the drift velocity, respectively. In eqs 1 and 2, μ is the fluid viscosity. The proportionality between the drag force and velocity may be expressed in terms of the drag coefficient c, i.e., $F = cV$. Equations 1 and 2 are applicable in the small Knudsen number limit, i.e., $\mathrm{Kn}_R = \lambda/R \ll 1$, where λ is the mean free path of the fluid.

For an NSB or a slender body in the free molecule regime ($\mathrm{Kn}_R = \lambda/R \gg 1$), expressions for aerodynamic drag were also available. Notably, Dahneke [26] carried out a gas-kinetic theory analysis and extended Epstein's theory for spheres [27] to bodies of arbitrary shapes. In his analysis, Dahneke considered rigid-body collision only and treated two types of momentum

transfer, i.e., the diffuse and specular scattering models as discussed in Millikan [28, 29]. In absence of dynamic rotational effects, Dahneke's drag force expression takes the form of

$$F = \sqrt{2\pi m_g kT} \left[\varphi + \left(2 - \frac{6-\pi}{4}\varphi \right) \sin^2\alpha \right] NR\mathcal{L}V \ , \tag{3}$$

where m_g is the molecular mass of the gas, k is the Boltzmann constant, T is the temperature, N is the gas number density, and φ is the momentum accommodation factor ($0 \le \varphi \le 1$). Here the two limiting φ values are 0 for specular scattering and 1 for diffuse scattering. In eq 3, α specifies the orientation of the NSB with respect to the drift velocity $\mathbf{V}$ ($\alpha = 0$ for the cylinder collinear with $\mathbf{V}$ and $\alpha = \pi/2$ for the cylinder perpendicular to $\mathbf{V}$). Equation 3 differs from eqs 1 and 2 because of the fundamental difference in the mechanism of momentum transfer. While in Stokes flow viscous dissipation of the fluid surrounding the slender body governs the drag, in free molecule regime the drag arises from momentum transfer of direct collisions between the fluid molecules and the cylinder surface. FIG 1 illustrates the dependency of the drag coefficient on the radius of cylinders of a constant aspect ratio $\mathcal{L}/R$. In the Stokes flow regime ($\text{Kn}_R \ll 1$), we expect the drag coefficient C to be independent of R or the drag force $F \propto R$, whereas in the free molecule regime ($\text{Kn}_R \gg 1$), C is proportional to R or $F \propto R^2$ in the rigid-body limit of collision.

Equation 3 has been the foundation in recent studies of the transport properties of NSBs. For example, Kim et al. [14] obtained an orientation-averaged electrical mobility expression and used it to determine the length of nanowires from electric mobility measurement. They showed that the mobility is a strong function of the wire orientation, which in turn, are dependent on the electric field strength and wire aspect ratio. Li et al. [30] considered the effect of cylinder rotation and obtained an expression for the orientation averaged drag force from Dahneke's expressions. TABLE 1 presents several drag force formulations relevant to the current discussion.

As discussed before, Dahneke's theory considers rigid-body collision only, yet the dynamics of collision and the resulting momentum transfer can be impacted by potential energy of

interactions between an NSB and the fluid molecules. In general the potential energy of interactions increases the collision cross section and hence the drag. The shaded areas of FIG 1 depict this effect. Previous studies have shown the effect of potential interactions to be significant for particles smaller than 10 nm in diameter [31-33]. For that size range, further complication many stem from changes in the dominant mode of molecular scattering. As the particle size is decreased to a few nanometers the collision evolves from diffuse to specular scattering [34, 35]. In general, diffuse scattering yields a drag larger than specular scattering (*cf*, FIG 1). These peculiarities ought to be applicable for matters of arbitrary shapes. For these reasons, Dahneke's expression can be inadequate when applied to NSBs as they approach the molecular size in at least one of its size dimensions.

Gas-phase transport properties have been treated with the Chapman-Enskog theory with spherical, isotropic potential functions [36]. For both near-spherical and non-spherical molecules the potential function of interactions has been historically described by an isotropic Lennard-Jones (LJ) 12-6 function [37-42]. The validity of this assumption was never examined in detail for non-spherical molecules. Considering that the LJ potential parameters used to model the binary diffusion coefficient are estimated customarily from measured viscosity [38-41], there is no theoretical reason to believe that the use of the LJ potential would lead to adequate predictions for gas diffusivity. Recent molecular dynamics evidence indeed suggests that the spherical potential assumption can be inaccurate [43, 44].

Recognizing the aforementioned problems, Wong et al. [45] treated the drag coefficient using axisymmetric potential and a gas-kinetic theory. Although the treatment was shown to predict a range of relevant data, it does not converge to Dahneke's rigid-body expressions. Specifically, a more precise treatment of the trajectory of a gas molecule undergoing specular scattering with the cylinder, as will be adopted here, should lead to zero momentum transfer along the axial direction of the cylinder and thus reproduce Dahneke's expression.

In this paper we carried out a comprehensive gas-kinetic theory analysis for drag force on NSBs in the perfect cylinder limit with the aspect ratio $\mathcal{L}/2R \gg 1$. The potential force of

interactions between the fluid molecules and the cylinder is described by a potential function. We are interested in free molecule flows with the effective Knudsen number $\text{Kn}_R \gg 1$. Following Epstein [27], we considered specular and diffuse scattering separately. It has been identified earlier that the origin of diffuse scattering is molecular adsorption/desorption on particle surface [34, 35], which is applicable to NSBs also. Drag force expressions are obtained for cylinders that undergo Brownian rotation and for those that align with the drift velocity. The validity of the theoretical expressions is examined against experimental mobility data available for carbon nanotubes.

II. GAS KINETIC THEORY ANALYSIS

In principle, the gas-kinetic theory analysis of drag on a cylinder is similar to that of spherical particles [31]. FIG 2 shows the coordinate system. A cylinder of radius R and length $\mathcal{L}$ ($\mathcal{L}/2R \gg 1$) undergoes motion in a fluid with an instantaneous velocity $\mathbf{V}$. The axis of the cylinder lies along the y-axis, and $\mathbf{V}$ is on the y-z plane at the attack angle α. Fluid molecules of random velocity $\mathbf{v}$ collide with a differential cylinder section of length $d\ell$ at the relative velocity $\mathbf{g} = \mathbf{v} - \mathbf{V}$ with the differential collision cross section equal to $d\ell \cdot db$, where b is the impact parameter. The velocity vector $\mathbf{g}$ may be defined by the polar angle ϕ and azimuthal angle θ. Furthermore, β is the angle between $\mathbf{g}$ and the z-axis, and ζ is the angle between $\mathbf{g}$ and the y-axis.

Gas is assumed to be in local equilibrium and its mass-center velocity is equal to zero. In this reference frame, the velocity distribution of the gas molecules is

$$f_v = N\left(\frac{m_g}{2\pi kT}\right)^{3/2} \exp\left(-\frac{m_g v^2}{2kT}\right), \tag{4a}$$

where v is the velocity of gas molecules. There are several important assumptions worthy to be mentioned before we start our derivation. When the cylinder is moving in a gas, the drag force is essentially the result of the momentum exchange between gas molecules and the cylinder upon

collisions. The drift velocity $\overline{V}$ is the time average of $\mathbf{V}$, which is expected to be substantially smaller than v or g. The relative velocity $\mathbf{g}$ has the distribution

$$f_g = N\left(\frac{m_r}{2\pi kT}\right)^{3/2} \exp\left[-\frac{m_r(\mathbf{g}+\overline{\mathbf{V}})^2}{2kT}\right], \qquad (4b)$$

where $m_r = m_g m_c / (m_g + m_c)$ is the reduced mass with m_c being the mass of the cylinder.

III. SPECULAR SCATTERING

We shall consider first the case in which the collision between the gas molecule and cylinder is elastic. We neglect the cylinder-end effect for now and treat only momentum transfer on the side of the cylinder body. The end effect shall be discussed later. For a gas molecule moving toward the cylinder with a relative, incident velocity $\mathbf{g}$ and impact parameter b, as shown in FIG 2(a), the x-z plane projection of its trajectory is depicted in FIG 2(b). Let $\mathbf{g}'$ be the molecular velocity after the collision, and $\mathbf{e}$ is a unit vector of $\mathbf{g}' - \mathbf{g}$. In this plane, we construct a frame in which axis $\mathbf{e}_3$ is parallel to the incident velocity $\mathbf{g}$, and the axis $\mathbf{e}_2$ is normal to both $\mathbf{e}_3$ and the axis of the cylinder.

We treat cylinders with lengths much longer than the range in which the gas-cylinder interaction takes place. Thus, a key assumption we make here is that the cylinder is infinitely long (with respect to the local gas-cylinder interaction potential). This assumption also implies that momentum transfer along the cylinder axis is negligible, and that $\mathbf{g}' - \mathbf{g}$ is equal to the difference of velocity components in the x-z plane. The above assumption is consistent with Dahneke's treatment in the rigid-body limit, which produces zero drag when $\mathbf{V}$ is collinear with the cylinder axis. The assumption is different from that of Wong et al. [45] who assumed the momentum exchange to be always zero in the direction perpendicular to the O'AC plane as shown in FIG 2. Such an assumption would lead to non-zero drag on the cylinder (or a fluid mechanical shear) when the drift velocity is collinear to the cylinder in the specular limit, which is not physical.

The scattering angle $\chi = \chi(\mathbf{g})$ is given by

$$\chi = \pi - 2b \int_{r_m}^{\infty} r^{-2} \left[1 - \frac{b^2}{r^2} - \frac{2\Phi(r)}{m_r \left(g_x^2 + g_z^2 \right)} \right]^{-1/2} dr \, , \tag{5}$$

where r_m is the closest distance of encounter between the approaching molecule and the axis of the cylinder. We shall retain the use of m_r here for generality. In eq 5, $\Phi(r)$ is the potential function between the molecule and particle, which we assume to be a function of the normal distance r only as discussed earlier.

In specular elastic collision, the magnitude of gas molecule velocity is equal before and after collision, i.e., $g = g'$. The relative velocity $\mathbf{g}'$ may be given as

$$\mathbf{g}' = \mathbf{g}_y + \left| \mathbf{g}_x + \mathbf{g}_z \right| \left(\cos \chi \mathbf{e}_3 - \sin \chi \mathbf{e}_2 \right) \, . \tag{6}$$

For a given impact parameter b the differential momentum transferred to the cylinder from the gas is

$$\mathbf{p} - \mathbf{p}' = m_r n \left(\mathbf{g} - \mathbf{g}' \right) = m_r n \left| \mathbf{g}_x + \mathbf{g}_z \right| \left[\left(1 - \cos \chi \right) \mathbf{e}_3 + \sin \chi \mathbf{e}_2 \right] \, , \tag{7}$$

in the cross section $d\ell \cdot db$ (FIG 2) over time dt. Here, ℓ is the shortest distance from the origin of the coordinate system to the O'AC plane (FIG 2). We note that the above equation shows that momentum transfer occurs only in the x-z plane as expected, and along the y-axis, the momentum transfer and force is zero. In eq 7, n is the number of molecules crossing $d\ell \cdot db$ over dt, i.e.,

$$n = g \cdot f_g \cdot d\ell \cdot db \cdot dt \, . \tag{8}$$

Note that upon integration, the term in the $\mathbf{e}_2$ direction vanishes. The total drag is the integral of the force in the $\mathbf{e}_3$ direction only over relative velocity $d\mathbf{g}$ and collision cross section $d\ell \cdot db$, i.e.,

$$
\begin{aligned}
\mathbf{F}_s &= \int_{\mathbf{g}} d\mathbf{F}_s = \int_{\mathbf{g}} \frac{\mathbf{p} - \mathbf{p}'}{dt} = \int_{\mathbf{g}} m_r n \left| \mathbf{g}_x + \mathbf{g}_z \right| \left(1 - \cos \chi \right) \mathbf{e}_3 \, d\mathbf{g} \\
&= \int_{\mathbf{g}} \int_{-\infty}^{\infty} \int_{-\mathcal{L}'/2}^{\mathcal{L}'/2} m_r g f_g \left| \mathbf{g}_x + \mathbf{g}_z \right| \mathbf{e}_3 \left(1 - \cos \chi \right) d\ell \, db \, d\mathbf{g}
\end{aligned} \tag{9}
$$

7

Define a collision integral $Q_{s,\perp} = Q_{s,\perp}(\mathbf{g})$ to be

$$Q_{s,\perp} = \int_{-\infty}^{\infty} \int_{-\mathcal{L}'/2}^{\mathcal{L}'/2} (1 - \cos\chi) d\ell\, db \ . \tag{10}$$

Here, the subscript "$\perp$" indicates that the drift velocity vector is perpendicular to the cylinder axis. The force expresion becomes

$$\begin{aligned}
\mathbf{F}_s &= \int_{\mathbf{g}} m_r g f_g |\mathbf{g}_x + \mathbf{g}_z| \mathbf{e}_3 Q_{s,\perp}\, d\mathbf{g} \\
&= m_r \int_{\mathbf{g}} g f_g (g_x \mathbf{i} + g_z \mathbf{k}) Q_{s,\perp}\, d\mathbf{g}
\end{aligned}, \tag{11}$$

where $\mathbf{i}$ and $\mathbf{k}$ are the unit vectors along the x and z axes. In eq 10, $\mathcal{L}'$ is the maximum distance beyond which potential force of gas-cylinder interaction becomes negligible. It is reasonable to argue that $\mathcal{L}'$ is proportional to the projection of the cylinder length on the plane perpendicular to $\mathbf{g}$. Thus we can write

$$\mathcal{L}' = \mathcal{L} w(g,b) \sin\zeta \ , \tag{12}$$

where ζ is the angle between $\mathbf{g}$ and the y axis (FIG. 2), and $w(g,b)$ is some function of g and b which is expected to be slightly larger than unity. Here we approximate $w(g,b) \cong 1$.

Since $g \gg \overline{V}$, the distribution function of g can be written as

$$\begin{aligned}
f_g d\mathbf{g} &= N \left(\frac{m_r}{2\pi kT} \right)^{3/2} \exp\left(-\frac{g^2 + \overline{V}^2 + 2g\overline{V}\cos\beta}{2kT/m_r} \right) dg_x dg_y dg_z \\
&\cong N \left(\frac{m_r}{2\pi kT} \right)^{3/2} \exp\left(-\frac{m_r g^2}{2kT} \right) \left(1 - \frac{m_r g \overline{V}\cos\beta}{kT} \right) dg_x dg_y dg_z
\end{aligned}. \tag{13}$$

Putting eq 13 into eq 11, we obtain

$$\begin{aligned}
\mathbf{F}_s = Nm_r &\left(\frac{m_r}{2\pi kT} \right)^{3/2} \int_{-\infty}^{\infty} \int_{-\infty}^{\infty} \int_{-\infty}^{\infty} g(g_x \mathbf{i} + g_z \mathbf{k}) Q_{s,\perp} \exp\left(-\frac{m_r g^2}{2kT} \right) \\
&\left(1 - \frac{m_r g \overline{V}\cos\beta}{kT} \right) dg_x dg_y dg_z
\end{aligned}. \tag{14}$$

The first term in $1 - m_r g V \cos\beta / kT$ vanishes upon integration, and thus

$$\mathbf{F}_s = -\frac{m_r N \bar{V}}{(2\pi)^{3/2}} \left(\frac{m_r}{kT}\right)^{5/2} \int_{-\infty}^{\infty}\int_{-\infty}^{\infty}\int_{-\infty}^{\infty} g^2 \left(g_x \mathbf{i} + g_z \mathbf{k}\right) Q_{s,\perp}$$
$$\cos\beta \exp\left(-\frac{m_r g^2}{2kT}\right) dg_x dg_y dg_z \tag{15}$$

It may be shown that the integral of the **i**-component is zero, and the net force is non-zero for the **k**-component or in the z direction. The coordinate system used has the z-component of the drift velocity ($\bar{\mathbf{V}}_\perp$) perpendicular to the cylinder axis. The corresponding force equation is

$$\mathbf{F}_s = -\frac{m_r N \bar{V}_\perp}{(2\pi)^{3/2}} \left(\frac{m_r}{kT}\right)^{5/2} \int_{-\infty}^{\infty}\int_{-\infty}^{\infty}\int_{-\infty}^{\infty} g g_z^2 Q_{s,\perp} \exp\left(-\frac{m_r g^2}{2kT}\right) dg_x dg_y dg_z . \tag{16}$$

Note that $\bar{V}_\perp = \bar{V} \sin\alpha$. The above equation may be expressed in the spherical coordinate as

$$\mathbf{F}_s = -\frac{m_r N \bar{V}_\perp}{(2\pi)^{3/2}} \left(\frac{m_r}{kT}\right)^{5/2} \int_0^{\infty}\int_0^{2\pi}\int_0^{\pi} g^5 Q_{s,\perp} \exp\left(-\frac{m_r g^2}{2kT}\right) \cos^2\phi \sin\phi \, d\phi \, d\theta \, dg . \tag{17}$$

Let $\gamma = g / \sqrt{2kT/m_r}$, we find the generalized expression for drag force on a cylinder undergoing drift as

$$\mathbf{F}_s = -\frac{2N \bar{V}_\perp}{\pi} \sqrt{\frac{2m_r kT}{\pi}} \int_0^{\infty}\int_0^{2\pi}\int_0^{\pi} \gamma^5 Q_{s,\perp} \exp\left(-\gamma^2\right) \cos^2\phi \sin\phi \, d\phi \, d\theta \, d\gamma . \tag{18}$$

We define here a reduced collision integral as

$$\Omega_{s,\perp}^{(1,1)*} = \frac{1}{2R\mathcal{L}} \int_0^{\infty}\int_0^{2\pi}\int_0^{\pi} \gamma^5 \exp\left(-\gamma^2\right) Q_{s,\perp} \cos^2\phi \sin\phi \, d\phi \, d\theta \, d\gamma . \tag{19}$$

The total force is then

$$\mathbf{F}_s = -\frac{4}{\pi} \sqrt{\frac{2m_r kT}{\pi}} \Omega_{s,\perp}^{(1,1)*} N\mathcal{L}R\bar{\mathbf{V}}_\perp = -\frac{4}{\pi} \sqrt{\frac{2m_r kT}{\pi}} \Omega_{s,\perp}^{(1,1)*} N\mathcal{L}R\bar{V} \sin\alpha \mathbf{k} . \tag{20}$$

Based on eq 20, the drag coefficient is thus

$$c_{s,\perp} = \frac{4}{\pi}\sqrt{\frac{2m_r kT}{\pi}} N \mathcal{L} R \Omega_{s,\perp}^{(1,1)*} \ . \tag{21}$$

It may be shown that for rigid-body collision, $\Omega_s^{(1,1)*} = \pi^2/2$. Noting that $m_g \cong m_r$, the corresponding drag coefficient is

$$c_{s,\perp} = 2\sqrt{2\pi m_g kT}\, N \mathcal{L} R \tag{22}$$

which is identical to the solution of Dahneke [26]. Hence, Dahneke's expression is a special case of the present result.

IV. DIFFUSE SCATTERING

We now consider the case of diffuse scattering where the molecule "reflects" randomly over the hemisphere above the plane tangent to the point of contact on the cylinder surface. The velocity distribution of the reflected molecules is Maxwellian, i.e.,

$$f'_g = 2N'\left(\frac{m_r}{2\pi kT}\right)^{3/2} \exp\left(-\frac{m_r g'^2}{2kT}\right) , \tag{23}$$

where $\mathbf{g}'$ is the velocity of the "reflected" gas molecule. In the $\mathbf{e}$ direction (normal to the side surface of the cylinder), $\mathbf{g}'$ must be positive (FIG 2). N' represents the number density of the "reflected" molecules, and its value may be determined from mass conservation. By assuming that the temperature of the scattered molecules is equal to that of the incidence, the rate of incident molecules crossing from the differential cross section $d\ell \cdot db$ onto a surface element $d\mathbf{A}$ on the side of the cylinder body can be written as

$$gf_g \cdot d\ell \cdot db = \int_{\mathbf{g}'} \left(\mathbf{g}' \cdot d\mathbf{A}\right) f'_g d\mathbf{g}' \ . \tag{24}$$

Combining eqs 23 and 24, we obtain

$$N' = \sqrt{\frac{\pi m_r}{2kT}} \frac{d\ell \cdot db}{dA} gf_g \ . \tag{25}$$

The momentum of the reflected molecules is

$$\mathbf{p}' = \int_{\mathbf{g}'} m_r \mathbf{g}' \left(\mathbf{g}' \cdot d\mathbf{A} \right) f' \ dt \, d\mathbf{g}' \ . \tag{26}$$

Putting eqs 23 through 25 into the above equation, we obtain

$$\mathbf{p}' = \frac{1}{2\pi} \left(\frac{m_r}{kT} \right)^2 f_g g \, d\ell \, db \, dt \int_{\mathbf{g}'} \mathbf{g}' \left(\mathbf{g}' \cdot d\mathbf{A} \right) \frac{1}{dA} \exp\left(-\frac{m_r g'^2}{2kT} \right) \ d\mathbf{g}' . \tag{27}$$

It can be shown that the integral portion of the above equation is $\sqrt{2} \left(kT \right)^{5/2} \left(\pi / m_r \right)^{3/2} \mathbf{e}$. Hence

$$\mathbf{p}' = \sqrt{\frac{\pi kT}{2m_r}} m_r g f_g \, d\ell \, db \, dt \, \mathbf{e}, \tag{28}$$

where $\mathbf{e}$ is the unit vector normal to $d\mathbf{A}$. Noting that the force component in the $\mathbf{e}_2$ direction vanishes upon integration, we write the equation as

$$\mathbf{F}_d = \int_{\mathbf{g}} d\mathbf{F}_d = \int_{\mathbf{g}} \frac{\mathbf{p} - \mathbf{p}'}{dt} = \int_{\mathbf{g}} \int_{-\infty}^{\infty} \int_{-\mathcal{L}'/2}^{\mathcal{L}'/2} m_r g f_g \left[\mathbf{g} + \sqrt{\frac{\pi kT}{2m_r}} \sin\left(\frac{\chi}{2} \right) \mathbf{e}_3 \right] d\ell \, db \, d\mathbf{g} \ . \tag{29}$$

Putting eq 4 into eq 29 and simplifying, we obtain the total force to be

$$\mathbf{F}_d = -\frac{m_r N \overline{V}}{\left(2\pi \right)^{3/2}} \left(\frac{m_r}{kT} \right)^{5/2} \int_{\mathbf{g}} \int_{-\infty}^{\infty} \int_{-\mathcal{L}'/2}^{\mathcal{L}'/2} g^2 \exp\left(-\frac{m_r g^2}{2kT} \right) \cos\beta$$
$$\left[\mathbf{g} + \sqrt{\frac{\pi kT}{2m_r}} \sin\left(\frac{\chi}{2} \right) \mathbf{e}_3 \right] d\ell \, db \, d\mathbf{g} \tag{30}$$

As shown in Fig 2, the cylinder axis and drift velocity define the *y-z* plane. Momentum exchange normal to this plane is, on average, zero due to symmetry. Equation 30 may be rewritten as

$$\mathbf{F}_d = -\frac{m_r N}{\left(2\pi \right)^{3/2}} \left(\frac{m_r}{kT} \right)^{5/2} \left[\begin{array}{l} \overline{\mathbf{V}}_{\|} \int_{\mathbf{g}} g \, g_y^2 \exp\left(-\frac{m_r g^2}{2kT} \right) Q_{d,\|} \, d\mathbf{g} \\ + \overline{\mathbf{V}}_{\perp} \int_{\mathbf{g}} g \, g_z^2 \exp\left(-\frac{m_r g^2}{2kT} \right) Q_{d,\perp} \, d\mathbf{g} \end{array} \right], \tag{31}$$

where $\bar{\mathbf{V}}_\parallel$ is the drift velocity component parallel to the cylinder axis, and the collision cross sections are given by

$$Q_{d,\parallel} = 2b_0 \mathcal{L}' \; , \tag{32}$$

$$Q_{d,\perp} = 2\int_0^{b_0} \int_{-\mathcal{L}'/2}^{\mathcal{L}'/2} \left\{ 1 + \left[\frac{\pi kT}{2m_r\left(g_z^2 + g_x^2\right)} \right]^{1/2} \sin\left(\chi/2\right) \right\} d\ell\, db$$
$$+ 2\int_{b_0}^{\infty} \int_{-\mathcal{L}'/2}^{\mathcal{L}'/2} \left(1 - \cos\chi\right) d\ell\, db \; . \tag{33}$$

In the above equations we define the critical impact factor b_0 to be a value below which the molecule undergoes contact collision where diffuse scattering dynamics prevail; and when $|b| > b_0$ the colliding molecule undergoes fly-by collision without physical contact with the cylinder surface [31]. Furthermore, eq 31 may be written as

$$\mathbf{F}_d = -\frac{4}{\pi}\sqrt{\frac{2m_r kT}{\pi}} N\mathcal{L}R\left(\Omega_{d,\parallel}^{(1,1)*}\bar{\mathbf{V}}_\parallel + \Omega_{d,\perp}^{(1,1)*}\bar{\mathbf{V}}_\perp \right) , \tag{34}$$

where the reduced collision integrals are defined as:

$$\Omega_{d,\parallel}^{(1,1)*} = \frac{1}{2R\mathcal{L}}\int_0^{\pi}\int_0^{2\pi}\int_0^{\pi} \gamma^5 \exp\left(-\gamma^2\right) Q_{d,\parallel} \sin^3\phi\sin^2\theta\, d\phi\, d\theta\, d\gamma \; , \tag{35}$$

$$\Omega_{d,\perp}^{(1,1)*} = \frac{1}{2R\mathcal{L}}\int_0^{\pi}\int_0^{2\pi}\int_0^{\pi} \gamma^5 \exp\left(-\gamma^2\right) Q_{d,\perp} \cos^2\phi\sin\phi\, d\phi\, d\theta\, d\gamma \; . \tag{36}$$

Alternatively the above equation can be written as

$$\mathbf{F}_d = -\left(c_{d,\parallel}\bar{\mathbf{V}}_\parallel + c_{d,\perp}\bar{\mathbf{V}}_\perp\right) , \tag{37}$$

where the drag coefficients are

$$c_{d,\parallel} = \frac{4}{\pi}\sqrt{\frac{2m_r kT}{\pi}} N\mathcal{L}R\Omega_{d,\parallel}^{(1,1)*} \; , \tag{38}$$

$$c_{d,\perp} = \frac{4}{\pi}\sqrt{\frac{2m_r kT}{\pi}} N\mathcal{L}R\Omega_{d,\perp}^{(1,1)*} \; , \tag{39}$$

We note that the current result differ from the earlier analysis of Wong et al. [45] again because of their assumption of zero momentum transfer in the direction perpendicular to the O'AC plane.

V. SCATTERING MODEL

We have discussed the two limiting models of molecular scattering upon impact with a slender body. Physically the scattering process falls between the two limits. In an earlier MD study [34], we explained the origin of inelastic diffuse scattering to be the result of transient molecular adsorption/desorption on the particle surface. The random walk following adsorption and the fact that desorption is the result of fluctuation cause the gas molecule to have little to no memory to its incident angle. This phenomenon occurs when a particle becomes large enough (typically a few nanometers in radius) and has enough internal degrees of freedom to accommodate the incident kinetic energy of the gas molecule. Another factor that contributes to an increased tendency of molecular adsorption is a reduced surface curvature as the particle becomes larger, leading to an increased probability of subsequent bounces and capture of the gas molecule following the initial impact. The MD simulation basically explained why molecular collisions are close to elastic specular (as exemplified by the success of the Chapman-Enskog theory in explaining molecular transport properties [36, 37]), and Millikan's observation [28, 29] that the drag measured for his oil droplets (> 0.03 μm) is more consistent with Epstein's theory of diffuse scattering [27]. In fact, Millikan proposed that his data was better explained by a 90% diffuse and 10% specular scattering mix, leading to a net force equal to $\mathbf{F} = 0.9\mathbf{F}_d + 0.1\mathbf{F}_s$. Here, the coefficient 0.9 is commonly known as the momentum accommodation factor [28].

Recognizing that the specular, elastic scattering must transit into diffuse scattering as a "particle" crosses over a certain size boundary, the momentum accommodation factor is, in fact, not a constant. For this reason, we introduced a momentum accommodation function φ [34, 35] ($0 \le \varphi \le 1$) and demonstrated the variation of φ with respect to particle size for several particle materials [35]. Following the earlier approach [32], we write the drag-force expression for a cylinder in a similar manner:

$$\mathbf{F} = \varphi \mathbf{F}_d + \left(1 - \varphi\right) \mathbf{F}_s \; . \tag{40}$$

As in the case of drag on spherical particles, the momentum accommodation function bears the greatest uncertainty. In section IX, we shall shed some light on this function using carbon nanotube as an example.

Combining eq 40 with eqs 20, 21 and 37, we obtain

$$\mathbf{F} = -\left\{ \left[\varphi c_{d,\perp} + \left(1 - \varphi\right) c_{s,\perp} \right] \bar{\mathbf{V}}_\perp + \varphi c_{d,\parallel} \bar{\mathbf{V}}_\parallel \right\} \; , \tag{41}$$

where $c_{s,\perp}$, $c_{d,\perp}$, $c_{d,\parallel}$ are given by eqs 21, 38 and 39, respectively, in which the collision integrals are reduced to

$$\Omega_s^{(1,1)*} = \pi^2 / 2$$
$$\Omega_{d,\perp}^{(1,1)*} = \pi^2 \left(6 + \pi\right) / 16$$
$$\Omega_{d,\parallel}^{(1,1)*} = \pi^2 / 4$$

for rigid-body collision. Substituting the above integral values into eqs 22, 38, and 39, expressing the drag force in terms of viscosity $\mu = N m_g \lambda \sqrt{2kT/\pi}$ and letting $m_g \cong m_r$ the force in the rigid-body limit is

$$\mathbf{F} = -\frac{\pi \mu \mathcal{L}}{Kn_R} \left[\varphi + \left(2 - \frac{6 - \pi}{4} \varphi \right) \sin^2 \alpha \right] \bar{\mathbf{V}} \; , \tag{42}$$

a result identical to that given by Dahneke [26].

VI. ROTATION AND CYLINDER ORIENTATION EFFECT

For cylinders with length substantially smaller than the mean free path of the gas, i.e., $Kn_{\mathcal{L}} = \lambda / \mathcal{L} \gg 1$ and in absence of a strong external force field that causes alignment of the cylinder axis with the drift velocity in any direction, the cylinder is expected to undergo unhindered rotation. Under this condition the cylinder orientation may be treated by a uniformly random distribution. As we persistently indicated in the derivation, the force expressions given thus far are the instantaneous force. This force does not always align with the drift velocity. It is

clear, however, that the force components perpendicular to the draft velocity must all vanish after orientation averaging. From eq 40, we may write the drag force as

$$\mathbf{F} = -\left\{ \left[\varphi c_{d,\perp} + (1-\varphi) c_{s,\perp} \right] \sin^2 \alpha + \varphi c_{d,\parallel} \cos^2 \alpha \right\} \bar{\mathbf{V}}. \tag{43}$$

Averaging over all solid angles ($0 \le \alpha \le \pi$ and $0 \le \xi \le 2\pi$), we find the average drag force on a freely rotating cylinder with $\mathrm{Kn}_R \gg \mathrm{Kn}_{\mathscr{L}} \gg 1$ to be

$$\begin{aligned} F_\odot &= \frac{\bar{V}}{4\pi} \int_0^{2\pi} \int_0^{\pi} \left\{ \left[\varphi c_{d,\perp} + (1-\varphi) k_{s,\perp} \right] \sin^2 \alpha + \varphi c_{d,\parallel} \cos^2 \alpha \right\} \sin \alpha \, d\alpha \, d\xi \\ &= \frac{1}{3} \left\{ 2 \left[\varphi c_{d,\perp} + (1-\varphi) c_{s,\perp} \right] + \varphi c_{d,\parallel} \right\} \bar{V} \end{aligned} \tag{44}$$

The above equation can be written equivalently following Li et al. [30, 46] as

$$F_\odot = \frac{1}{3} \left(c_x + c_y + c_z \right) \bar{V} \tag{45}$$

where c_x, c_y and c_z are the drag-coefficient components in along the *x*, *y* and *z*-axes, respectively,

$$c_x = c_z = \varphi c_{d,\perp} + (1-\varphi) c_{s,\perp} \tag{46}$$

$$c_y = \varphi c_{d,\parallel} \, . \tag{47}$$

In other words, the total drag force is the sum of contributions along each major axis when the cylinder can undergo free rotation.

VII.   CYLINDER WITH SPHERICAL END CAPS

Almost all nano-cylinders have end caps that can be approximated as half spheres of diameter $2R$. Again in the limit of $\mathrm{Kn}_R \gg \mathrm{Kn}_{\mathscr{L}} \gg 1$, the drag force may be written as

$$F_\odot = \frac{1}{3} \left\{ 8 \sqrt{2\pi m_r kT} \, N R^2 \Omega_{s/d,sph}^{(1,1)*} + 2 \left[\varphi c_{d,\perp} + (1-\varphi) c_{s,\perp} \right] + \varphi c_{d,\parallel} \right\} \bar{V} \tag{48}$$

where the first term represents the drag force on the end cap, which is equal to that of a sphere. The expressions for $\Omega_{sph,s/d}^{(1,1)*}$ have been given in Li and Wang [31, 32]. Suffice it to note that if

the end cap effect is considered the overall length of the cylinder is $\mathcal{L} + 2R$ and the calculation of $c_{d,\perp}$, $c_{s,\perp}$ and $c_{d,\parallel}$ should use the length of the cylindrical section of the cylinder ($\mathcal{L}$), and not $\mathcal{L} + 2R$.

VIII.   FICKIAN DIFFUSIVITY OF CHAIN-LIKE MOLECULES

Orientation-averaged aerodynamic drag in the form of eq 44 may be re-cast into Fickian diffusivity in dilute gases via the Einstein-Smoluchowski relation [47], $D = kT/c$. Typical long-chain molecules have lengths substantially shorter than the mean free path of the gas and can undergo free rotation in dilute gases. As an example, normal hexadecane has a length of approximately 2 nm. In comparison the mean free path of ambient air is around 70 nm.

The diffusion coefficient of a long-chain molecule l in a dilute bath gas g may be approximated from eq 44:

$$D_{l,g} = \frac{3kT}{2\left[\varphi c_{d,\perp} + \left(1 - \varphi\right)c_{s,\perp}\right] + \varphi c_{d,\parallel}}. \tag{49}$$

Following the Chapman-Enskog treatment, we assume specular collision ($\varphi = 0$) and obtain

$$D_{l,g} = \frac{3kT}{2c_{s,\perp}} = \frac{3\pi}{8}\sqrt{\frac{\pi kT}{2m_r}}\frac{1}{N\mathcal{L}R\Omega_{s,\perp}^{(1,1)*}}. \tag{50}$$

The validity of the above equation will be examined in a separate study [48], but the equation is shown to differs from the Chapman-Enskog (C-E) expression, as expected, since the C-E equation is applicable for spherical potential only.

If the end-cap effect is considered, the diffusion coefficient takes an expanded form

$$D_{l,g} = \frac{3\pi}{8}\sqrt{\frac{\pi kT}{2m_r}}\frac{1}{NR\left(\mathcal{L}\Omega_{s,\perp}^{(1,1)*} + \pi^2 R\Omega_{s,sph}^{(1,1)*}\right)}. \tag{51}$$

16

IX. REDUCED COLLISION INTEGRALS AND ELECTRIC MOBILITY OF CNTS

In the limiting collision models we have three relevant, reduced collision integrals as given by eqs 19, 35 and 36. They are dependent on the potential energy of gas-cylinder interactions. For a given cylinder material and bath molecule, the reduced collision integrals are a function of the cylinder radius, as expected. In principle, the integrals approach the respective values of the rigid-body limit as the cylinder radius is increased. Conversely, the deviation from the rigid-body limit increases as the cylinder radius is decreased due to an enhanced effect of van der Waals interactions on the cross section relative to the cylinder diameter. This effect is identified as the non-rigid body effect towards small cylinder radius as shown in FIG 1.

Consider the transport of a carbon nanotube (CNT) in air. The potential function of interaction has been given by Wong et al. [45] as

$$\Phi(r*) = a_0 R^{m+1} \sigma^{1-m} n_c \varepsilon \left(a_1 r *^{-n_1} - a_2 r *^{-n_2} \right) , \tag{52}$$

where σ and ε are the Lennard-Jones (LJ) 12-6 collision diameter and well depth between carbon and the bath molecule, respectively, n_c is the surface density of carbon ($n_c = 0.381$ Å^{-2}), $r*$ is the normalized, shortest distance of the gas molecule to the CNT surface,

$$r* = (r - R)\big/\sigma . \tag{53}$$

In eq 52 the constants are given as $a_0 = 5.81$, $m = -0.86$, $a_1 = 0.635$, $a_2 = 1.63$, $n_1 = 10.1$, and $n_2 = 4.1$ [45]. The potential function equation was derived from a sum for the pairwise interactions of carbons in a CNT with a bath molecule with the LJ 12-6 potential function. Here, we adopted the values of Wong et al. for the LJ parameters: $\sigma = 3.576$ Å and $\varepsilon/k = 58.7$ K [45], which were based on the LJ self-collision parameters of carbon and molecular nitrogen and the mixing rule $\sigma_{12} = (\sigma_1 + \sigma_2)\big/2$ and $\varepsilon_{12} = (\varepsilon_1 \varepsilon_2)^{1/2}$.

FIG 3 shows the variations of the reduced collision integrals computed as a function of the cylinder radius using the above potential function. For all cases the reduced collision integrals approach their respective, rigid-body limits at $1\big/(2R) = 0$ or $R \to \infty$ (the open circles of the Figure). Deviations from the rigid-body limits indicate the influence of the potential force of

interaction on the collision cross section. For small-diameter tubes the non-rigid body effect is very significant. Compared to rigid body collision the collision cross section is enhanced by as much as a factor of 2 due to the potential energy of interactions. These observations indicate a rigid-body approximation can be grossly inaccurate. Additionally, the reduced collision integral appears to be roughly linear in $1/R$ for a wide range of cylinder radii. The intercept corresponds to the rigid-body limit. The linear dependency is expected because the difference in the reduced collision integral between non rigid-body and rigid-body collisions is proportional to δ/R, where δ measures the increase in the collision cross section due to the potential force of interaction. This potential force is local relative to the cylinder size. This leads to the fact that δ is basically independent of R, and hence, the linear dependency with respect to $1/R$.

Differential mobility analyzer (DMA) is instrumental to our ability to characterize a wide range of aerosols of nanomaterials of different shapes and sizes [49]. For spherical particles in the large Knudsen number limit the Stokes-Cunningham expression [50, 51] is traditionally used to interpret the mobility data, giving what is known as the mobility particle diameter,

$$D_m = \frac{q}{3\pi\mu Z}\left\{1 + \mathrm{Kn}\left[A + B\exp\left(-E/Kn\right)\right]\right\} . \tag{55}$$

Previous studies [31, 32] have shown that the above expression with coefficients A, B and E fitted to Millikan's oil droplet data [28, 52, 53] gives a reasonably good estimate for small particle sizes, but owing to its empirical nature, an extrapolation below the smallest size of Millikan's oil droplets can lead to some errors. The problem arises from an increased effect of potential energy of gas-phase interaction as the particle approaches the molecular size [35].

Mobility can also provide partial information about the size of non-spherical nanomaterials of a known shape. Several studies [12, 14, 16, 20, 30, 54-57] have reported data of CNT mobility measured by a DMA, among them the relationship between the mobility diameter and CNT length is provided for a given tube diameter. For some of the CNTs, the length and

diameter were determined directly by transmission electronic microscopy (TEM). These data will be used here to examine the validity of the current theory.

The mobility of a CNT is influenced by several factors. They include the orientation of the nanotube with respect to the electric field and hence the drift velocity, the potential energy of gas-CNT interactions, and the momentum accommodation factor. During DMA measurement, CNTs are first charged ($q = \pm 1$). The aerosol is sent into an electric field with strength ranging from 0.4 to 5 kV/cm. The interaction of the charge with the electric field and the polarization of the CNT produce a torque that tends to align it along the direction of the external electric field. In the DMA, the electric field is parallel to the drift velocity. Kim et al. [14] calculated the electrostatic force due to the net charge in the CNT by assuming that the positive charge is located at the end of the CNT closest to the negative electrode. The torque is proportional to the length of the CNT. As for interaction caused by the dielectric charge, they proposed a complex function of the torque with respect to the cylinder volume and aspect ratio. The theory predicts that long CNTs align with the electric field, while short CNTs tend to assume uniform random orientations. Hence we expect to observe a transition from randomly distributed orientations to the collinear orientation at some CNT length. By assuming the probability of the orientation angle follows a Boltzmann-like distribution (i.e., eq 10 of [14]) and integrating it over all orientations, we may extend eq 44 and write a drag force that depends on the orientation probability as:

$$F_{eff} = \frac{\bar{V}}{4\pi} \int_0^{2\pi} \int_0^{\pi} \left\{ \left[\varphi c_{d,\perp} + (1 - \varphi) c_{s,\perp} \right] \sin^2 \alpha + \varphi c_{d,\parallel} \cos^2 \alpha \right\} P_\alpha d\alpha d\xi, \qquad (56)$$

where P_α is given by eq 24 of Kim et al. [58]. The corresponding orientation-averaged electric mobility can be obtained accordingly:

$$Z_{eff} = \frac{4\pi q}{\int_0^{2\pi} \int_0^{\pi} \left\{ \left[\varphi c_{d,\perp} + (1 - \varphi) c_{s,\perp} \right] \sin^2 \alpha + \varphi c_{d,\parallel} \cos^2 \alpha \right\} P_\alpha d\alpha d\xi}, \qquad (57)$$

where $c_{s,\perp}$, $c_{d,\parallel}$ and $c_{d,\perp}$ are given by eqs 22, 38 and 39, respectively. All of these coefficients may be determined for a tube of radius R and length $\mathcal{L}$, if the potential function parameters are known, as discussed above for CNTs (eq. 52). Additionally, the distribution function P_α and orientation-averaged electric mobility is also a function of the electric mobility and the aspect ratio of the cylinder. The equivalent mobility diameter of a CNT may be calculated by replacing Z in eq 55 by Z_{eff}.

FIG 4 shows the length-versus-mobility diameter data of CNTs, all of which are 15 nm in diameter and taken from several sources [12, 30, 54, 55]. In this set of data, the CNT diameter was determined by TEM, while the length ($\mathcal{L}$) was estimated from the TEM projected area (A_p) as $\mathcal{L} = A_p/(2R)$. The projected area was obtained from direct TEM measurement or an empirical correlation developed for A_p as a function of the mobility diameter D_m [55]. In the figure, the data corresponding to directly measured projected area are marked as solid symbols, and those from the corelation are marked as open symbols.

The theoretical mobility and thus mobility diameter can be calculated in two limiting orientations of the CNT with repsect to the direction of the drift velocity. In the collinear and random orientation limits and neglecting the CNT end effect, the mobility is given by

$$Z_\parallel = \frac{q}{\varphi c_{d,\parallel}} = \frac{1}{\varphi \Omega_{d,\parallel}^{(1,1)*}} \frac{\pi q}{4\sqrt{\frac{2m_r kT}{\pi}} N \mathcal{L} R} \tag{58}$$

$$Z_\odot = \frac{3q}{2\left[\varphi c_{d,\perp} + (1-\varphi)c_{s,\perp}\right] + \varphi c_{d,\parallel}}$$
$$= \frac{1}{2\left[\varphi \Omega_{d,\perp}^{(1,1)*} + (1-\varphi)\Omega_{s,\perp}^{(1,1)*}\right] + \varphi \Omega_{d,\parallel}^{(1,1)*}} \frac{3\pi q}{4\sqrt{\frac{2m_r kT}{\pi}} N \mathcal{L} R}, \tag{59}$$

The above mobility may be converted to the mobility diameter via eq 55. Also, for a given R value, the tube length $\mathcal{L}$ values may be determined from eqs 57 and 58 for the collinear and random orientations, respectively. As shown in FIG 4, the experimental data are bracketed between the theoretical values of the two limiting orientations. Here, we used a momentum

accommodation factor of 1.0. We observe here that the length of the longest CNT shown is outside the collinear orientation limit. In fact, a φ value of 0.85 to 0.9 can predict that particular data point rather well. These values are also inline with what was observed for spherical particles as discussed in Millikan [29]. Here we shall not adopt a non-unity φ value based on just one data point, except to say that for CNTs 15 nm in diameter, the data clearly show that the momentum accommodation factor is close to unity. It can be seen from the figure that the longest tubes ($\mathcal{L} > 1000$ nm) is collinear with the electric field in the DMA (and thus the drift velocity) and the orientation of the shortest tube ($\mathcal{L} \sim 130$ nm) is random and uniformly distributed with respect to the electric field.

CNT lengths between the two limits may be predicted using eq 57 from measured electric mobility (or mobility diameter) and CNT diameter. The result is shown as the dotted line in FIG 4. Clearly, transition from uniform random orientation to collinear orientation takes place in the length range shown; and the current theory of nanocylinder transport combined with the orientation distribution function proposed by Kim et al. [14] reproduce the data satisfactorily in that length range. This agreement extends to CNTs of different diameter values. In FIG 5, we plot the reduced collision integrals of a series of CNTs 10, 15, and 22 nm in diameter as a function of their measured lengths. The data are taken from several relevant sources [12, 30, 55]. The measured mobility Z, the length of $\mathcal{L}$ and diameter $2R$ of each CNT may be converted to an experimentally determined reduced collision integral via

$$\Omega^{(1,1)*}_{\text{expt}} = \frac{\pi q}{4\sqrt{\frac{2m_r kT}{\pi}}\, N \mathcal{L} RZ} \,, \tag{60}$$

The above experimental collision integral may be compared to theoretical predictions in the collinear and random orientation limits (shown as the grey band in FIG 5):

$$\Omega^{(1,1)*}_{\text{eff},\parallel} = \varphi\, \Omega^{(1,1)*}_{d,\parallel} \,, \tag{61}$$

$$\Omega_{\text{eff},\odot}^{(1,1)*} = 2\left[\varphi\, \Omega_{d,\perp}^{(1,1)*} + \left(1-\varphi\right)\Omega_{s,\perp}^{(1,1)*} \right] + \varphi\, \Omega_{d,\parallel}^{(1,1)*} . \tag{62}$$

with $\varphi = 1$, as discussed before. Additionally, an effective reduced collision integral may be defined from eq 57 to account for CNT orientation distributions and thus the transition from random orientation distribution to collinear orientation. Clearly, within the range of CNT diameter considered, the short tubes have randomly distributed orientations with respect to the drift velocity, the long tubes align with the drift velocity. Again, the current theory combined with Kim et al.'s orientation distribution function describes the experimental data very well.

A previous study [35] indicates that for spherical particles below 10 nm in particle diameter the momentum accommodation φ decreases from approximately unity to zero as the particle size is decreased. That is, the collision becomes specular as the particle size approaches the molecular size. As discussed in Li and Wang [32], the transition from diffuse to specular scattering as the particle approaches the molecular size is entirely expected. Millikan's experiments on oil droplets yielded $\varphi = 0.9$ for >20 nm droplets; the specular elastic assumption of the Chapman-Enskog theory is extremely successful in predicting molecular transport. Thus, between the size of 20 nm and the molecular size, φ must undergo transition from unity to zero.

It is therefore possible that small-diameter CNTs assume a substantially smaller value for momentum accommodation. The mobility diameter (D_m) of small-diameter CNTs ($2R < 5$ nm) have been studied by Chiang et al. [54] and Unrau et al. [57]. In particular, Unrau et al. directly measured the length and electric mobility for several CNTs 2 nm in diameter over a CNT length range of ~100 to 1000 nm. In Fɪɢ 6 we compare the predicted lengths to the experimental length. Based on Kim's expression of the orientation distribution function of CNTs in an electric field, the CNTs examined should mostly assume random orientations. As shown in Fɪɢ 6 a momentum accommodation value of zero gives substantially better prediction of the data than $\varphi = 1$. Therefore, in addition to the demonstration that the current theory predicts availlable experimental data satisfactorily, the results shown in Fɪɢs 4 through 6 indicate that the diffuse-to-specular transition occur also for a CNTs as its diameter is reduced from 10 to 2 nm in a

manner entirely consistent with conclusions reached in previous analysis of spherical particles [32, 35].

X.   CONCLUSION

We obtained generalized expressions of the aerodynamic drag force on a cylinder in the free-molecule flow with a consideration of intermolecular interactions. The derivations are carried out using gas kinetic theory. Specular and diffuse scattering are discussed separately and the effect of the orientation of the cylinder is also considered in detail. The drag forces for specular and diffuse scattering take the same formulations although the cross sections are expressed separately. The effect of gas-cylinder interaction force is embedded in the collision integrals. The validity of the theoretical expressions is verified against the experimental mobility data of carbon nanotubes. It was shown that the potential energy of interactions is critical to describing the collision cross section and thus the drag on carbon nanotubes of diameter as large as 20 nm.

XI. REFERENCES

[1]   G. Kasper, T. Niida and M. Yang, J. Aerosol Sci. **16**, 535 (1985).

[2]   P. A. Baron, Ind. Health **39**, 39 (2001).

[3]   Z. Wang, P. K. Hopke, P. A. Baron, G. Ahmadi, Y. S. Cheng, G. J. Deye and W. C. Su, Aerosol Sci. Technol. **39**, 1056 (2005).

[4]   B. T. Chen, H. C. Yeh and C. H. Hobbs, Aerosol Sci. Technol. **19**, 109 (1993).

[5]   B. T. Chen, H. C. Yeh and N. F. Johnson, J. Aerosol Sci. **27**, 83 (1996).

[6]   G. J. Deye, P. Gao, P. A. Baron and J. Fernback, Aerosol Sci. Technol. **30**, 420 (1999).

[7]   K. B. Shelimov, D. E. Clemmer, R. R. Hudgins and M. F. Jarrold, J. Am. Chem. Soc. **119**, 2240 (1997).

[8]   M. F. Jarrold, Ann. Rev. Phys. Chem. **51**, 179 (2000).

[9]   D. E. Clemmer and M. F. Jarrold, J. Mass Spectrom. **32**, 577 (1997).

[10] M. Dimaki and P. Bøggild, Nanotechnol. **15**, 1095 (2004).

[11] B. Edwards, N. Engheta and S. Evoy, J. Appl. Phys. **102**, 024913 (2007).

[12] S. H. Kim and M. R. Zachariah, Nanotechnol. **16**, 2149 (2005).

[13] S. H. Kim and M. R. Zachariah, J. Phys. Chem. B **110**, 4555 (2006).

[14] S. H. Kim, G. W. Mulholland and M. R. Zachariah, J. Aerosol Sci. **38**, 823 (2007).

[15] A. D. Maynard, P. A. Baron, M. Foley, A. A. Shvedova, E. R. Kisin and V. Castranova, J. Toxicol. Env. Heal. A **67**, 87 (2004).

[16] A. Moisala, A. G. Nasibulin, S. D. Shandakov, H. Jiang and E. I. Kauppinen, Carbon **43**, 2066 (2005).

[17] A. Moisala, A. G. Nasibulin, D. P. Brown, H. Jiang, L. Khriachtchev and E. I. Kauppinen, Chem. Eng. Sci. **61**, 4393 (2006).

[18] A. G. Nasibulin, A. Moisala, D. P. Brown, H. Jiang and E. I. Kauppinen, Chem. Phys. Lett. **402**, 227 (2005).

[19] D. K. Song, I. W. Lenggoro, Y. Hayashi, K. Okuyama and S. S. Kim, Langmuir **21**, 10375 (2005).

[20] C. J. Unrau, R. L. Axelbaum, P. Biswas and P. Fraundorf, in *Molecular Building Blocks for Nanotechnology: From Diamondoids to Nanoscale Materials adn Applications*, edited by G. A. Mansoori *et al.* (Springer, New York, 2007), pp. 212.

[21] A. J. Smallbone, W. Liu, C. K. Law, X. Q. You and H. Wang, Proc. Combust. Inst. **32**, 1245 (2009).

[22] A. T. Holley, X. Q. You, E. Dames, H. Wang and F. N. Egolfopoulos, Proc. Combust. Inst. **32**, 1157 (2009).

[23] C. Ji, E. Dames, Y. L. Wang, H. Wang and F. N. Egolfopoulos, Combust. Flame **157**, 277 (2010).

[24] G. K. Batchelor, J. Fluid Mech. **44**, 419 (1970).

[25] R. G. Cox, J. Fluid Mech. **44**, 791 (1970).

[26] B. E. Dahneke, J. Aerosol Sci. **4**, 147 (1973).

[27] P. S. Epstein, Phys. Rev. **23**, 710 (1924).

[28] R. A. Millikan, Phys. Rev. **21**, 217 (1923).

[29] R. A. Millikan, Phys. Rev. **22**, 1 (1923).

[30] M. Li, G. W. Mulholland and M. R. Zachariah, Phys. Rev. E **89** (2014).

[31] Z. Li and H. Wang, Phys. Rev. E **68**, 061206 (2003).

[32] Z. Li and H. Wang, Phys. Rev. E **68**, 061207 (2003).

[33] Z. Li and H. Wang, Phys. Rev. E **70**, 021205 (2004).

[34] Z. Li and H. Wang, Phys. Rev. Lett. **95**, 014502 (2005).

[35] H. Wang, Ann. N. Y. Acad. Sci. **1161**, 484 (2009).

[36] T. G. Cowling and S. Chapman, *The mathematical theory of non-uniform gases* (University Press, 1960).

[37] J. O. Hirschfelder, C. F. Curtiss and R. B. Bird, *Molecular Theory of Gasses and Liquids* (Wiley, New York, 1954).

[38] T. R. Marrero and E. A. Mason, J. Phys. Chem. Ref. Data **1**, 3 (1972).

[39] J. Kestin, K. Knierim, E. A. Mason, B. Najafi, S. T. Ro and M. Waldman, J. Phys. Chem. Ref. Data **13**, 229 (1984).

[40] A. Boushehri, J. Bzowski, J. Kestin and E. A. Mason, J. Phys. Chem. Ref. Data **16**, 445 (1987).

[41] J. Bzowski, J. Kestin, E. A. Mason and F. J. Uribe, J. Phys. Chem. Ref. Data **19**, 1179 (1990).

[42] R. C. Reid, J. M. Prausnitz and B. E. Poling, (1987).

[43] K. Chae, P. Elvati and A. Violi, J. Phys. Chem. B **115**, 500 (2010).

[44] K. Chae and A. Violi, J. Chem. Phys. **134**, 044537 (2011).

[45] R. Y. Wong, C. Liu, J. Wang, C. Y. Chao and Z. Li, J. Nanosci. Nanotechno. **12**, 2311 (2012).

[46] M. Li, R. You, G. W. Mulholland and M. R. Zachariah, Aerosol Sci. Technol. **47**, 1101 (2013).

[47] A. Einstein, Ann. Phys. (Berlin) **324**, 371 (1906).

[48] C. Liu, W. C. McGivern, J. A. Manion and H. Wang, J. Chem. Phys. **Manuscript in preparation** (2016).

[49] H. G. Scheibel and J. Porstendo, J. Aerosol Sci. **14**, 113 (1983).

[50] E. Cunningham, Proc. Royal Soc. Lon. Ser.-A **83**, 357 (1910).

[51] M. Knudsen and S. Weber, Ann. Phys. (Berlin) **341**, 981 (1911).

[52] R. A. Millikan, Science, 436 (1910).

[53] R. A. Millikan, Philos. Mag. **34**, 1 (1917).

[54] W. H. Chiang and R. M. Sankaran, Diam. Relat. Mater. **18**, 946 (2009).

[55] S. H. Kim, G. W. Mulholland and M. R. Zachariah, Carbon **47**, 1297 (2009).

[56] C. J. Unrau, R. L. Axelbaum, P. Biswas and P. Fraundorf, Proc. Combust. Inst. **31**, 1865 (2007).

[57] C. J. Unrau and R. L. Axelbaum, Carbon **48**, 1418 (2010).

[58] S. Kim, G. Mulholland and M. Zachariah, J. Aerosol Sci. **38**, 823 (2007).

TABLE I. Selected drag force formulations for cylindrical body

| Author(s)	Drag force expression	Comments
Cox [25]	$$F_{\parallel} = 2\pi\mu\mathcal{L}V\left[\frac{1}{\ln\left(\mathcal{L}/R\right)-3/2-\ln 2}+O\left\{\frac{1}{\left[\ln\left(\mathcal{L}/R\right)\right]^3}\right\}\right]$$ $$F_{\perp} = 4\pi\mu\mathcal{L}V\left[\frac{1}{\ln\left(\mathcal{L}/R\right)-1/2+\ln 2}+O\left\{\frac{1}{\left[\ln\left(\mathcal{L}/R\right)\right]^3}\right\}\right]$$	Circular cylinder of length $\mathcal{L}$ at rest in a uniform fluid flow of velocity **V**. The solution is obtained in *Stokes flows* neglecting the inertia effect.
Dahneke [26]	$$F = \sqrt{2\pi m_g kT}\left[\varphi+\left(2-\frac{6-\pi}{4}\varphi\right)\sin^2\alpha\right]NR\mathcal{L}\bar{V}$$ $$= \frac{\pi\mu\mathcal{L}}{Kn_R}\left[\varphi+\left(2-\frac{6-\pi}{4}\varphi\right)\sin^2\alpha\right]\bar{V}$$ $$c_{d,\parallel}=\frac{\pi\varphi\mu\mathcal{L}}{Kn_R}\text{ for }\alpha=0\text{ (collinear).}$$ $$c_{d,\perp}=\left(2-\frac{6-\pi}{4}\varphi\right)\frac{\pi\mu\mathcal{L}}{Kn_R}\text{ for }\alpha=\pi/2\text{ (perpendicular)}$$	Drag force on a cylinder in the *free molecule regime* with rigid body collision. Mixed scattering is expressed by the momentum accommodation factor $0\le\varphi\le 1$, where the two limits are specular scattering and diffuse scattering, respectively.
Kim et al. [14]	$$F=\frac{\pi\mu\mathcal{L}\bar{V}}{Kn_R}\left[\varphi+\left(2-\frac{6-\pi}{4}\varphi\right)\langle\sin^2\alpha\rangle\right]$$	An extension of Dahneke's solution by treating cylinder rotation; $\langle\sin^2\alpha\rangle$ is the mean of $\sin^2\alpha$ which may be determined from the distribution function of attack angle.
Li et al. [30]	$F=3\left(1/c_{d,\parallel}+2/c_{d,\perp}\right)^{-1}\bar{V}$ for slow Brownian rotation relative to translational relaxation; $F=\frac{1}{3}\left(c_{d,\parallel}+2c_{d,\perp}\right)\bar{V}$ for fast Brownian rotation relative to translational relaxation.	$c_{d,\parallel}$ and $c_{d,\perp}$ are drag coefficients as given by Dahneke's solutions [26].
This work	$$F_{\odot}=\frac{1}{3}\left\{2\left[\varphi c_{d,\perp}+(1-\varphi)c_{s,\perp}\right]+\varphi c_{d,\parallel}\right\}\bar{V}$$ $$F_{\parallel}=\varphi c_{d,\parallel}\bar{V}$$ where $$c_{d,\parallel}=\frac{4}{\pi}\sqrt{\frac{2m_r kT}{\pi}}N\mathcal{L}R\Omega_{d,\parallel}^{(1,1)*}$$ $$c_{d,\perp}=\frac{4}{\pi}\sqrt{\frac{2m_r kT}{\pi}}N\mathcal{L}R\Omega_{d,\perp}^{(1,1)*}$$ $$c_{s,\perp}=\frac{4}{\pi}\sqrt{\frac{2m_r kT}{\pi}}N\mathcal{L}R\Omega_s^{(1,1)*}$$	$F_{\odot}$ and $F_{\parallel}$ are drag forces on cylinders in uniformly random orientation and parallel to drift velocity, respectively. The reduced collision integrals $\Omega^{(1,1)*}$ accounts for the non-rigid body effect. Their expressions can be found in the text.
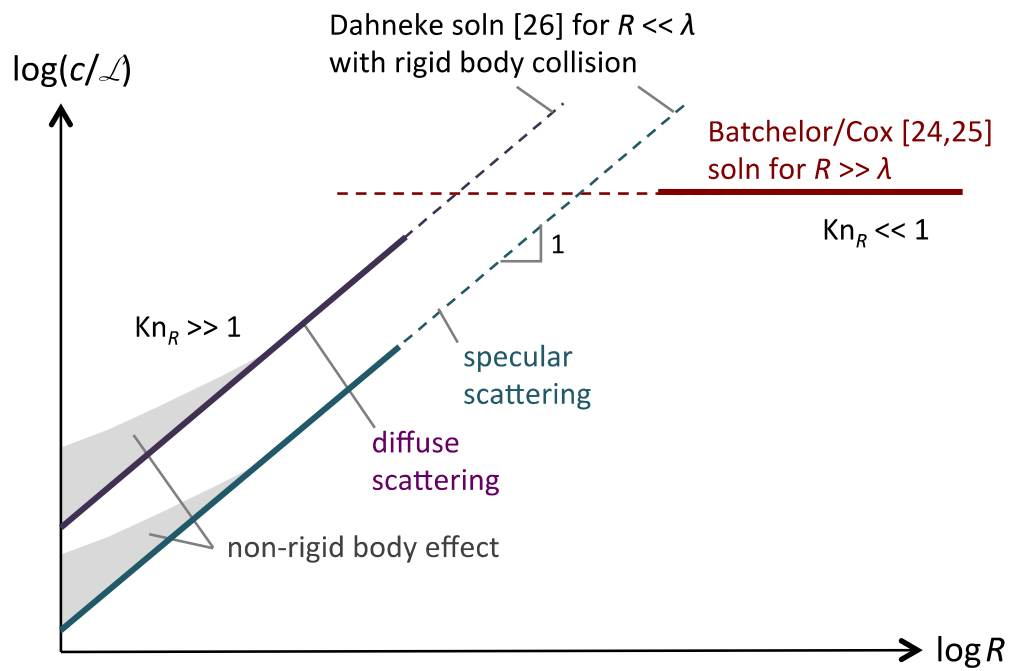
FIG 1. Schematic illustration of the limiting solutions of specific drag coefficient ($c/\mathcal{L}$) of cylinders of a constant aspect ratio $\mathcal{L}/(2R) \gg 1$. The Batchelor-Cox solution is for Stokes flow ($Kn_R \ll 1$) and the Dahneke solution is applicable to free molecule regime ($Kn_R \gg 1$).
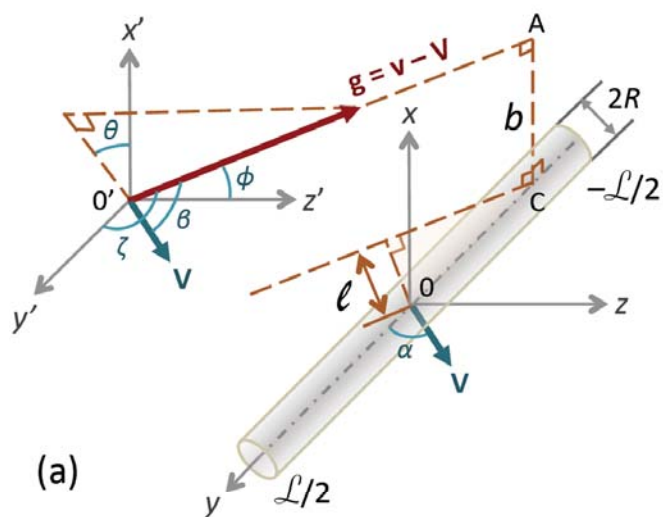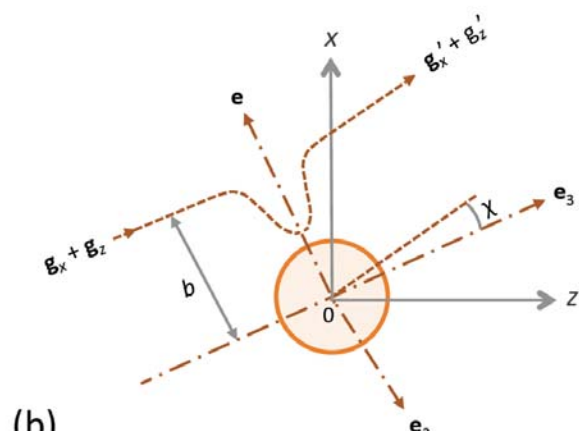
FIG 2. (a) schematic of the coordinate system; (b) x-z plane projection of the collision trajectory of the molecule. $\mathbf{g}_x + \mathbf{g}_z$ and $\mathbf{g}'_x + \mathbf{g}'_z$ are the molecular velocity components in the x-z plane before and after collision, respectively, and χ is the scattered angle.

29
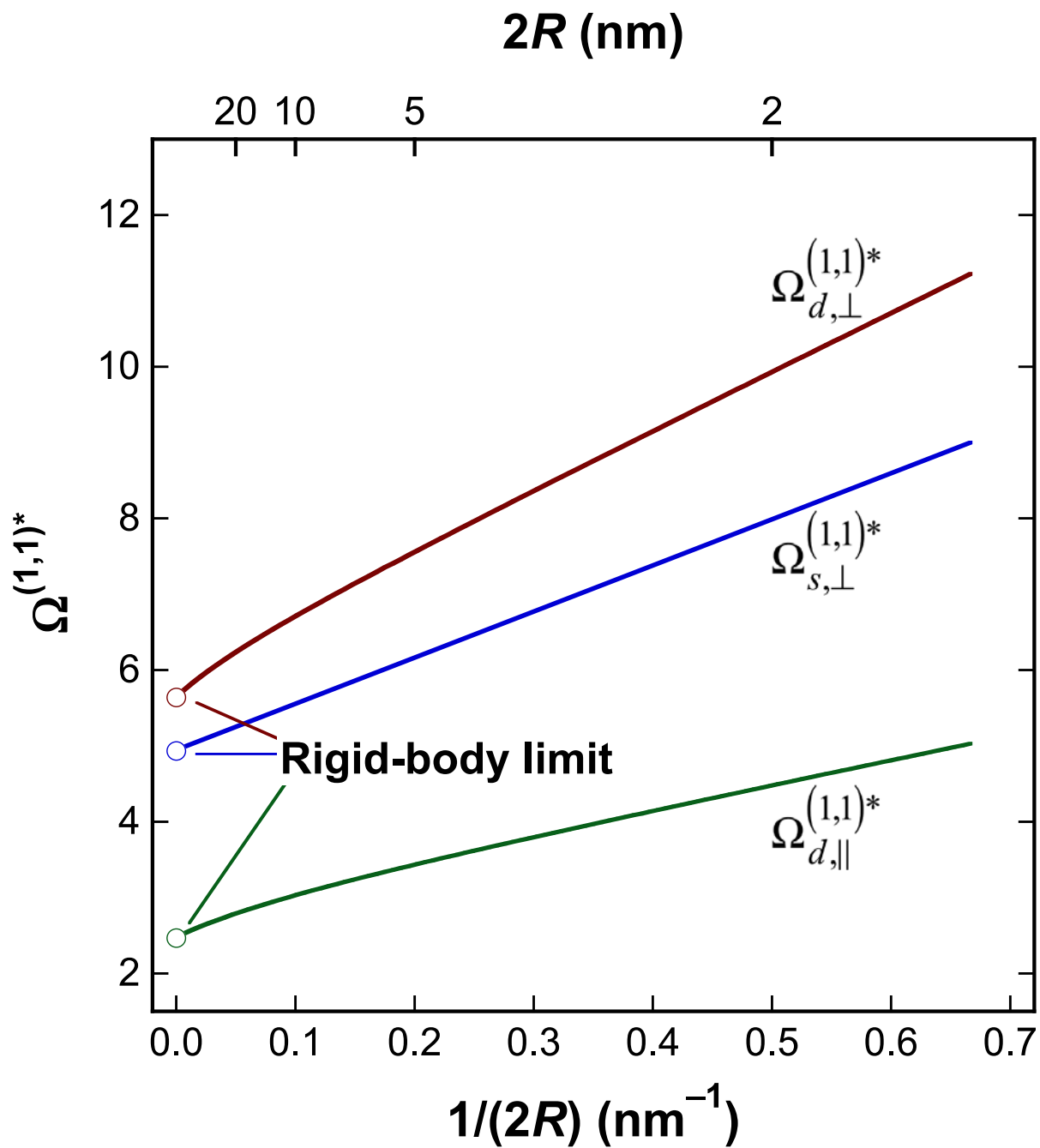
FIG 3. Reduced collision integrals (solid lines) as a function of cylinder radius computed for carbon nanotube and molecular nitrogen at 298 K. The open circles denote reduced collision integrals equivalent to rigid-body collision.
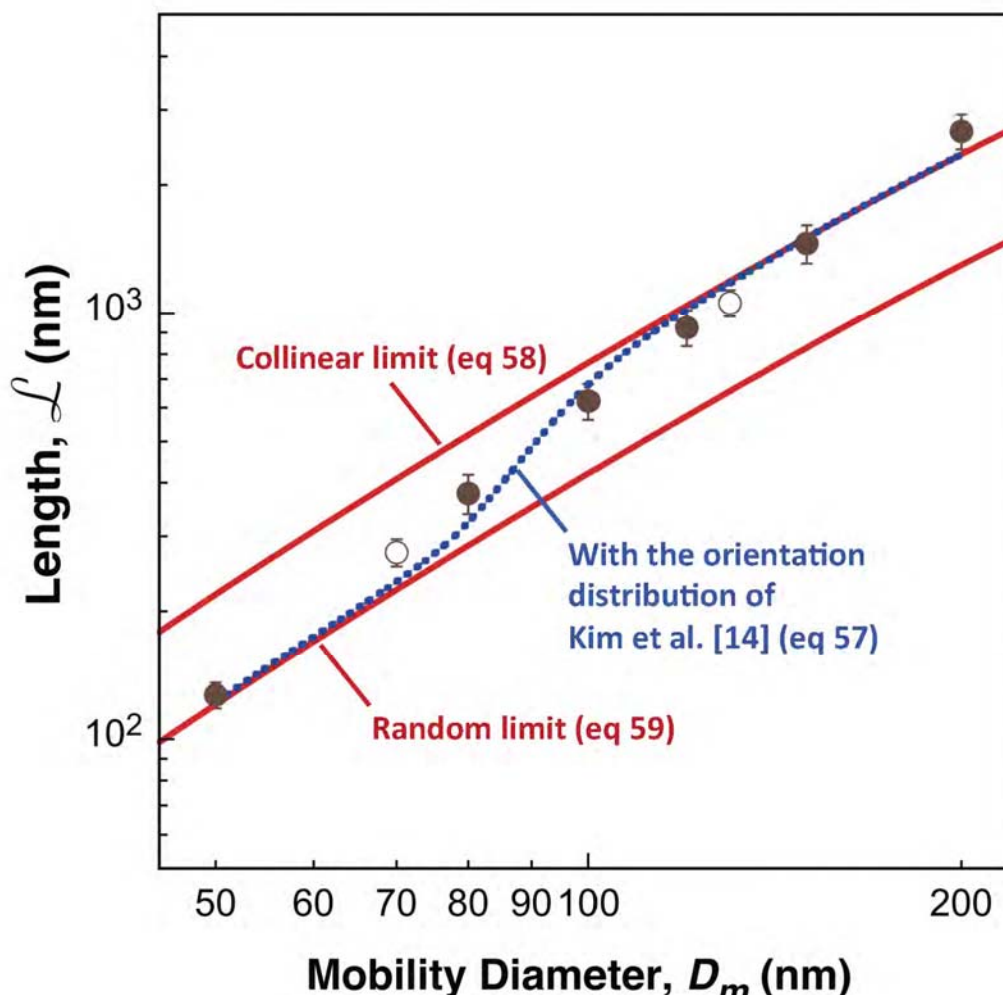
FIG 4. Length of CNTs 15 nm in diameter as a function of the mobility diameter measured in air at 1 bar and 298 K. Symbols: experimental data taken from [12, 30, 55] (solid symbols: directly measured; open symbols: from the experimental correlation between mobility diameter and TEM projected area [55]); solid lines: theoretical predictions using the momentum accommodation factor $\varphi = 1$, in two limiting CNT orientations with respect to the drift velocity (electric field); dotted lines: theoretical predictions accounting for orientation angle distribution of the CNT in the electric field [14].
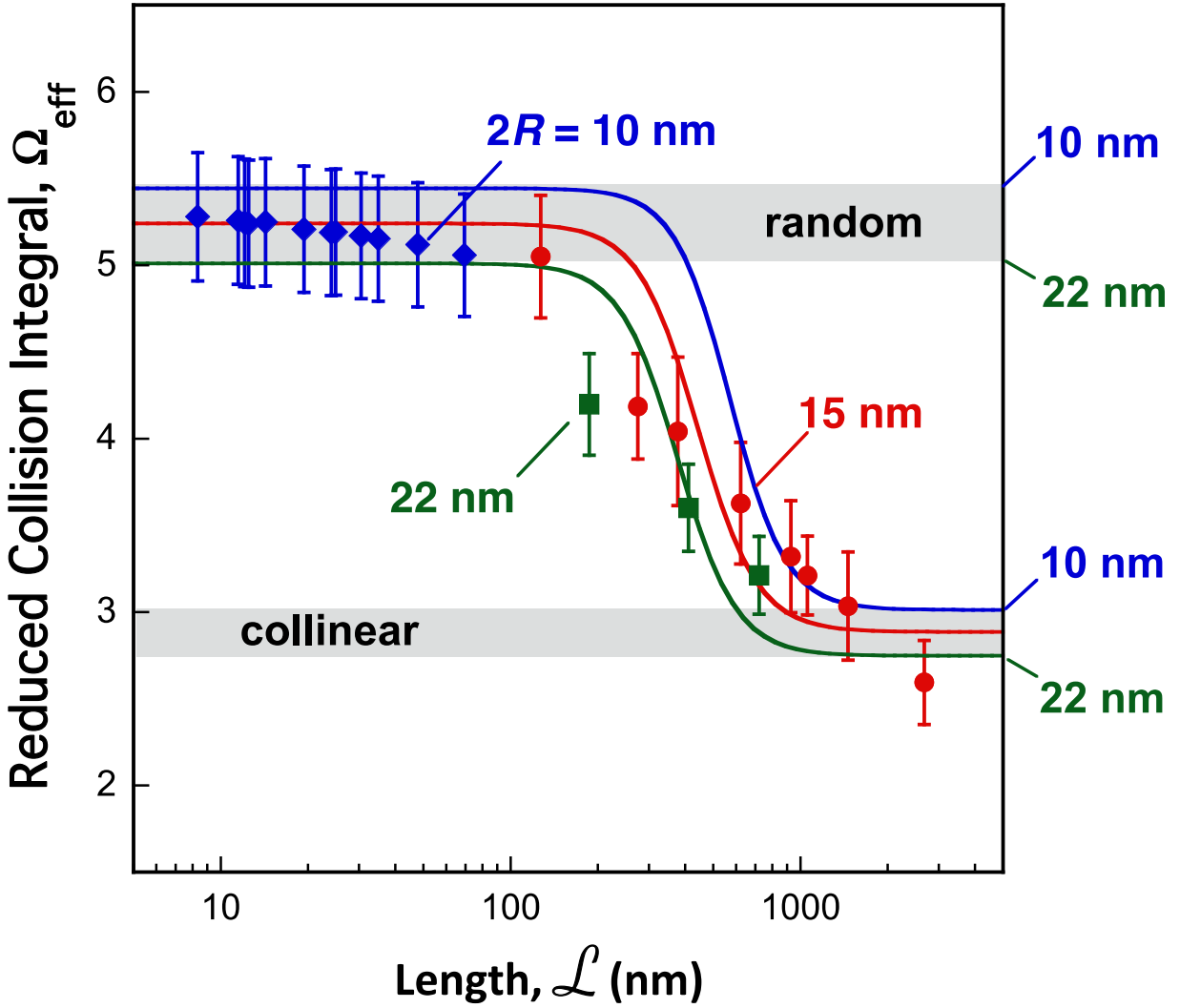
FIG 5. Reduced collision integrals derived from the CNT mobility data for $2R = 10$ nm [54] and $2R = 15$ and 22 nm [12, 30, 55] as a function of the CNT length (symbols). The error bars for $2R = 15$ and 22 nm data are taken from the reference sources directly, while those for $2R = 10$ nm are estimated to be 10%, based on a TEM resolution of 0.5 nm for CNT diameter determination. The theoretical predictions are shown in the random and collinear orientations of CNTs with respect to the drift velocity with $\varphi = 1$ for the momentum accommodation factor (grey bands). Lines are theoretical predictions accounting for orientation angle distribution of the CNT in the electric field [14].
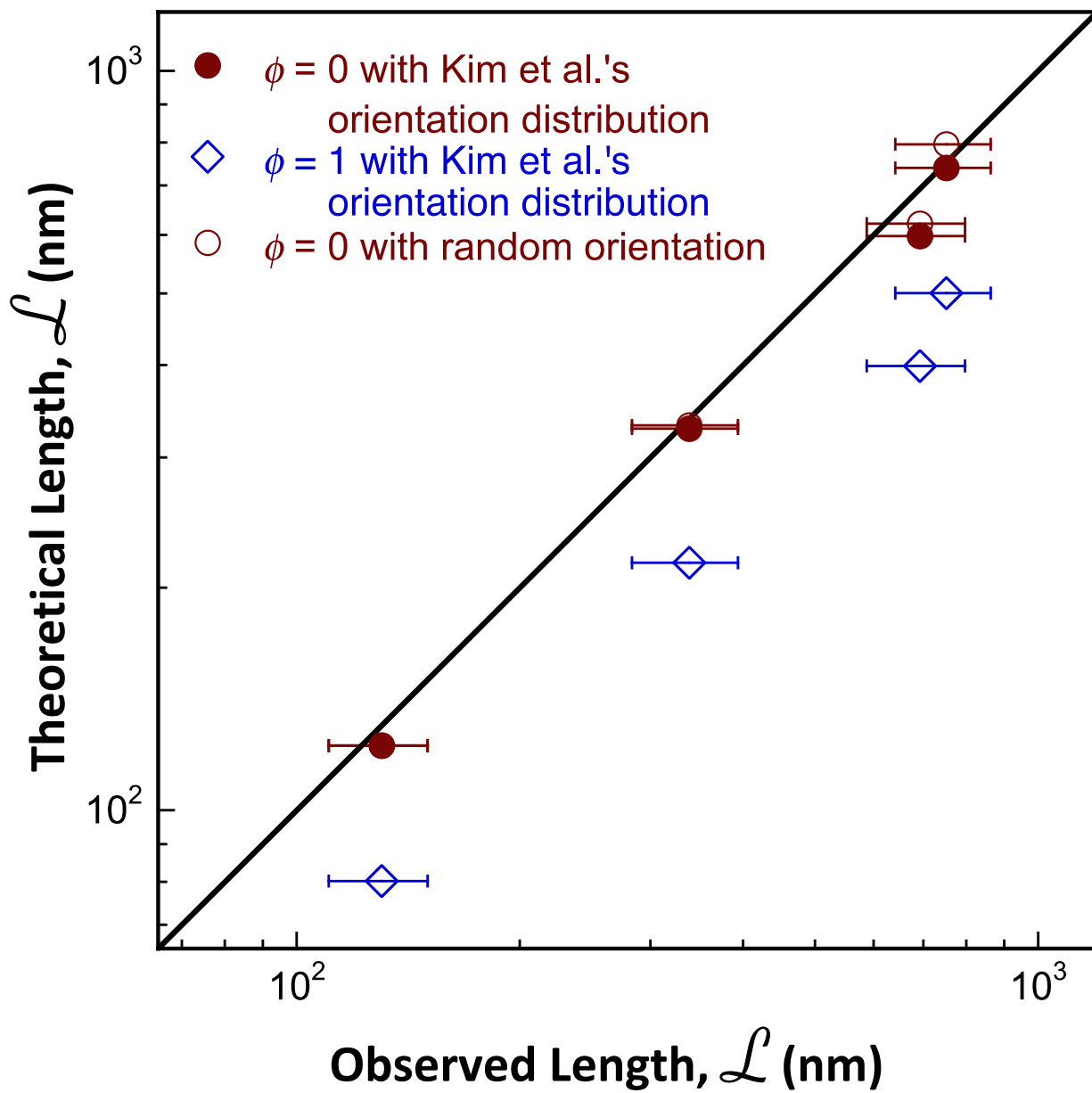
FIG 6. Comparison of predicted and observed length of CNTs 2 nm in diameter. The experimental data are taken from Unrau et al. [57].